mor frequencies, $\Omega \gg \omega$, and the field is "high" so that $\Omega\tau \gg 1$, where τ is the correlation time of the dipole term. When the former condition holds and more generally when the dipole rates are small compared with $1/\tau + 1/T_e$, Eqs. (B13)–(B16) can be solved by iteration. Thus the familiar expressions from the I-spin relaxation are obtained by putting $p = 0$ as the argument of $\bar{f}^L_{\alpha\mu}$ in Eqs. (B13) and (B15), and the first-order corrections to the S-spin relaxation follow from (B14) and (B16) by taking $p = -1/T_{2e}$ and $p = -1/T_{1e}$ in $\bar{f}^L_{\alpha\mu}$, respectively. In order to apply the Eqs. (B10) and (B13)–(B16) to an inhomogeneous system, they must, in principle, first be solved for p which is then to be averaged over an appropriate ensemble for the values of C and τ. In the above approximation this amounts to averaging the equations, which makes this case indistinguishable (as far as relaxation is concerned) from the case of a homogeneous system with a non-exponential correlation function.

---

*Work based on a thesis submitted to the Faculté des Sciences de Paris, 1969 (unpublished).

[1]J. Leblond, P. Papon, and J. Korringa, preceding paper, Phys. Rev. A4, 1532 (1971), hereafter referred to as Paper I.

[2]P. Papon, thesis (Paris University, 1967) (unpublished); P. Papon, J. L. Motchane, and J. Korringa, Phys. Rev. 175, 641 (1968).

[3]A similar distribution was needed in order to account for the proton relaxation in the pure solvents.

[4]A. Yoshimori and J. Korringa, Phys. Rev. 128, 1054 (1962).

[5]J. Korringa, Phys. Rev. 133, A1228 (1964).

[6]J. Korringa, J. L. Motchane, P. Papon, and A. Yoshimori, Phys. Rev. 133, A1230 (1964).

[7]C. D. Jeffries, *Dynamic Nuclear Orientation* (Interscience, New York, 1963), p. 123.

[8]E. H. Poindexter and J. Uebersfeld, J. Chem. Phys. 36, 2706 (1962); E. H. Poindexter, *ibid.* 43, 3587 (1965). 3587 (1965).

[9]J. L. Motchane and P. Papon, Phys. Rev. 141, 246 (1966).

PHYSICAL REVIEW A VOLUME 4, NUMBER 4 OCTOBER 1971

High-Frequency Electrostatic Plasma Instabilities

J. P. Freidberg and B. M. Marder
University of California, Los Alamos Scientific Laboratory, Los Alamos, New Mexico 87544
(Received 14 October 1970; revised manuscript received 30 April 1971)

A description of the stability properties of a plasma under the influence of an external electric field oscillating near the plasma frequency is presented.

I. INTRODUCTION

We investigate the stability properties of a homogeneous plasma under the influence of an alternating electric field oscillating at frequencies near the plasma frequency. Describing the stability properties of this system represents a first step in the understanding of a mechanism for absorption of energy in a plasma from laser radiation. This problem has been studied by many authors[1–6] using various analytic expansion techniques. The basic results of their work have been the discovery of two distinct instabilities which occur when the driving frequency is either slightly above or below the Bohm-Gross frequency. It is our aim in this paper to consolidate and expand upon their work by solving the equations numerically, thereby obtaining solutions for a wide range of parameters. From these results it is possible to obtain a relatively simple picture of the structure of the two fundamental unstable modes.

II. THEORY

In the collisionless approximation the equations governing the behavior of a homogeneous plasma under the influence of an electric field

$$\vec{E}_{ext} = \hat{y} E_0 \sin\omega_0 t$$

are

$$\frac{\partial f_j}{\partial t} + v\frac{\partial f_j}{\partial y} + \frac{q_j}{m_j} E \frac{\partial f_j}{\partial v} = 0 ,$$
$$\frac{\partial E}{\partial y} \equiv -\frac{\partial^2 \phi}{\partial y^2} = \frac{1}{\epsilon_0} \sum_j q_j \int f_j \, dv , \tag{1}$$

where j is e for electrons and i for ions. The oscillating solution about which we linearize is given by $f_j = f_j(v_j^*)$, where

$$v_j^* = v + (q_j E_0/m_j\omega_0)\cos\omega_0 t \equiv v + v_j^0 .$$

We shall take f_j to be a Maxwellian:

$$f_j(v_j^*) = (N_0/\pi^{1/2} v_{Tj}) \exp[-(v^*/v_{Tj})^2] .$$

We consider perturbations of the form

$$Q(y, v, t) = Q(v, t) e^{iky} .$$

After linearizing, substituting, and solving for the perturbed distribution function by integrating back along unperturbed orbits we obtain the following integral equation first obtained by Silin[1]:

$$\psi(t) + \int_0^\infty sH(s,t)\psi(t-s)\,ds = 0\,, \tag{2}$$

where $\psi(t)$ is related to the potential $\phi(t)$ by

$$\psi(t) = \phi(t)\exp\left[\frac{ikeE_0}{2\omega_0^2}\left(\frac{m_i - m_e}{m_i m_e}\right)\sin\omega_0 t\right]$$

and

$$H(s,t) = \sum_{j=i,e}\omega_{pj}^2\exp\left[-\left(\frac{kv_{Tj}s}{2\omega_0}\right)^2 - \frac{ikq_jE_0}{2\omega_0^2}\left(\frac{m_i+m_e}{m_i m_e}\right)\left[\sin\omega_0(t-s) - \sin\omega_0 t\right]\right].$$

III. COLD CASE

We first consider the limit in which $v_{Te} = v_{Ti} = 0$. It can be shown that the integral Eq. (2) reduces to the set of coupled second-order ordinary differential equations

$$\frac{d^2\rho_i}{dt^2} + \omega_{pi}^2\left(\rho_i - \rho_e e^{-ikL\sin\omega_0 t}\right) = 0\,, \tag{3}$$

$$\frac{d^2\rho_e}{dt^2} + \omega_{pe}^2\left(\rho_e - \rho_i e^{ikL\sin\omega_0 t}\right) = 0\,, \tag{4}$$

where

$$L = (eE_0/\omega_0^2)\left((m_i+m_e)/m_i m_e\right)$$

is a scale length related to particle excursions produced by the electric field E_0. ρ_e and ρ_i are related to the perturbed densities n_j by

$$\rho_{e,i} = n_{e,i}\exp\left(i\int_0^t kv_{e,i}^0\,dt\right).$$

Silin[1] has derived these equations using a fluid model.

Equations (3) and (4) are a fourth-order linear system with periodic coefficients and as such Floquet[7] theory can be used to obtain stability behavior. Briefly, the solutions and growth rates are computed as follows: We write Eqs. (3) and (4) as a system of four first-order equations $\dot{\vec{z}} = A\vec{z}$, where $A(t)$ is the periodic 4×4 matrix

$$A(t) = \begin{bmatrix} 0 & 0 & 1 & 0 \\ 0 & 0 & 0 & 1 \\ -\omega_{pi}^2 & \omega_{pi}^2 e^{-i\chi} & 0 & 0 \\ \omega_{pe}^2 e^{i\chi} & -\omega_{pe}^2 & 0 & 0 \end{bmatrix}$$

and $\chi = kL\sin\omega_0 t$. $\vec{z}$ is a four vector given by

$$\vec{z} = \begin{bmatrix} \rho_i \\ \rho_e \\ \dot{\rho}_i \\ \dot{\rho}_e \end{bmatrix}.$$

We calculate a fundamental solution matrix $Z(2\pi/\omega_0)$ by numerically integrating Eqs. (3) and (4) from 0 to $2\pi/\omega_0$ for four independent initial conditions. Here $Z(t) = [\vec{z}(1)\vec{z}(2)\vec{z}(3)\vec{z}(4)]$, where $\vec{z}(I)$ is the solution vector $\vec{z}(t)$ evaluated at time t for the Ith independent initial condition. Since A is periodic in $2\pi/\omega_0$, if $Z(t)$ is a solution to Eq. (3), then $Z(t+2\pi/\omega_0)$ is also a solution. Thus, it follows that

$$Z(t+2\pi/\omega_0) = Z(t)\Omega\,,$$

where Ω is a constant matrix. The stability of the system is determined by the eigenvalues of Ω. If we denote the four eigenvalues by λ_i then the growth rate of any given mode is

$$\gamma_i/\omega_0 = (1/2\pi)\ln|\lambda_i|\,.$$

Two properties of the λ_i can be easily ascertained. From the fact that the trace $(A) = 0$, it follows that $\lambda_1\lambda_2\lambda_3\lambda_4 = 1$. From Eqs. (1) and (2), we note that if $\rho(t)$ is a solution then $\rho^*(-t)$ is also a solution. This leads to the conclusion that the λ_i are either purely real or else occur in complex conjugates. In the numerical computations $Z(0)$ is taken to be the identity matrix. The computations were done for various values of m_e/m_i, kL, and ω_p/ω_0, where $\omega_p = (\omega_{pe}^2 + \omega_{pi}^2)^{1/2}$. An over-all picture of the stability

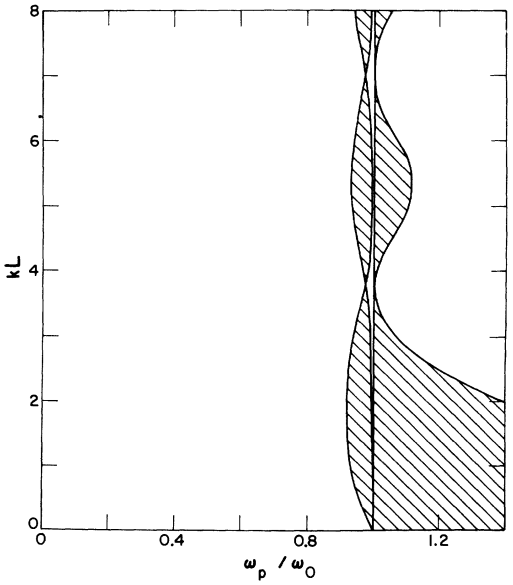

FIG. 1. Stable (clear) and unstable (cross-hatched) regions in the $(\omega_p/\omega_0, kL)$ plane.

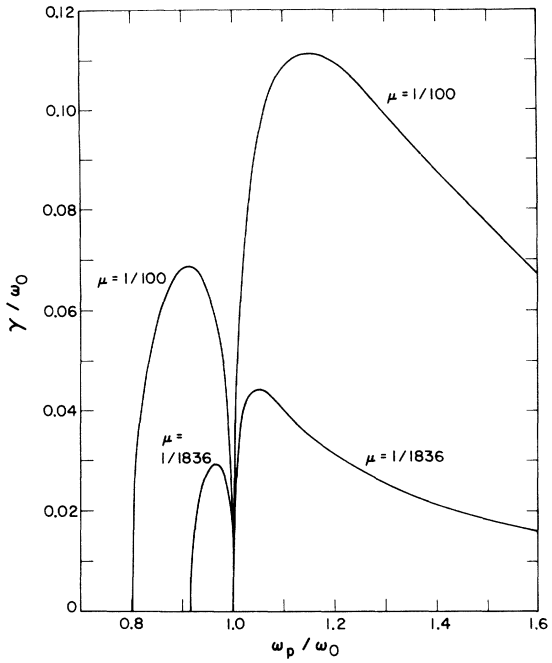

FIG. 2. Maximum growth rates vs ω_p/ω_0 for mass ratios of $\frac{1}{100}$ and $\frac{1}{1836}$.

of the system is given in Fig. 1, which is a plot of stable and unstable regions in $(\omega_p/\omega_0, kL)$ space for a fixed mass ratio $m_e/m_i = \frac{1}{1836}$. We see that

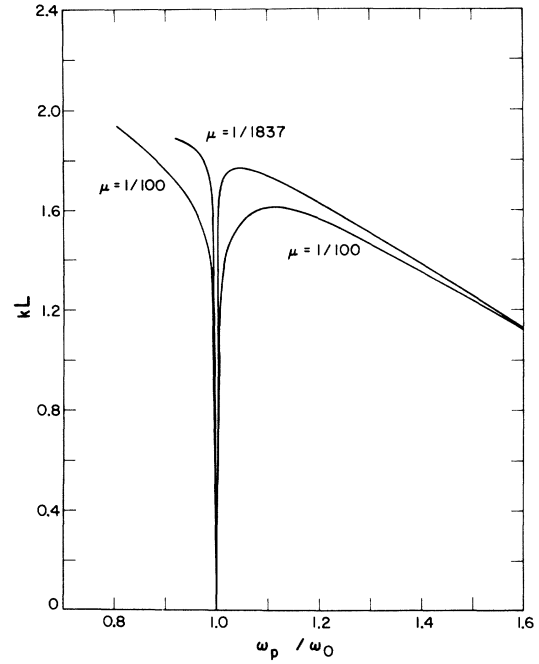

FIG. 3. Wave numbers corresponding to maximum growth vs ω_p/ω_0 for mass ratios of $\frac{1}{100}$ and $\frac{1}{1836}$.

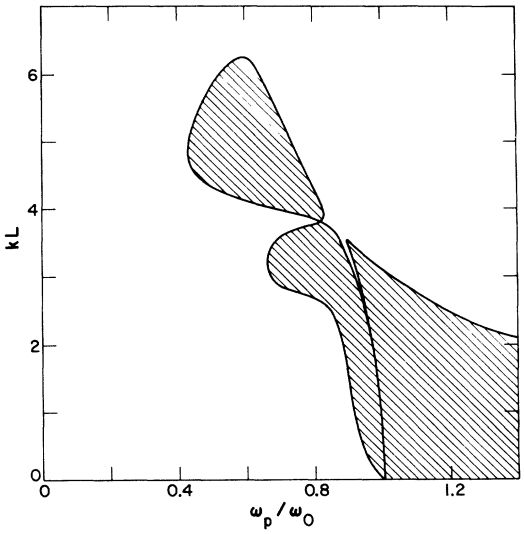

FIG. 4. Stability behavior for $v_{Te}/\omega_0 L = 0.1$ and $T_i/T_e = 0.1$.

for sufficiently high frequencies the system is stable. There is a significant region of instability in the underdense region and it appears that these instabilities exist for kL arbitrarily large. $\omega_0 = \omega_p$ is the transition point between what is usually referred to as the parametric (underdense) instability and the modified two-stream (overdense) instability. The nature of the eigenvalues λ is different in these two regions. In the underdense case $\mathrm{Im}\lambda_i \neq 0$, while in the overdense case $\mathrm{Im}\lambda_i$ is identically zero. In Figs. 2 and 3 we illustrate the maximum growth rate and corresponding wave number vs ω_p/ω_0 for mass ratios of $\frac{1}{100}$ and $\frac{1}{1836}$. The growth rates for the instability in the underdense region are substantial. This is significant with respect to the laser problem since this region feels the full intensity of the laser. Thus, the instabilities generated there may provide an efficient means of depositing laser energy into the plasma.

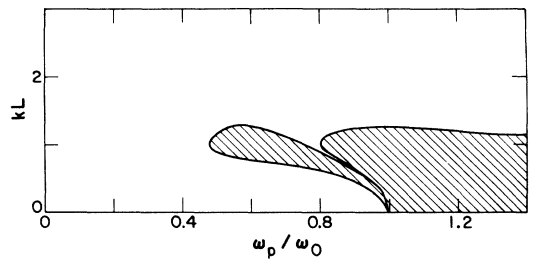

FIG. 5. Stability behavior for $v_{Te}/\omega_0 L = 0.5$ and $T_i/T_e = 0.1$.

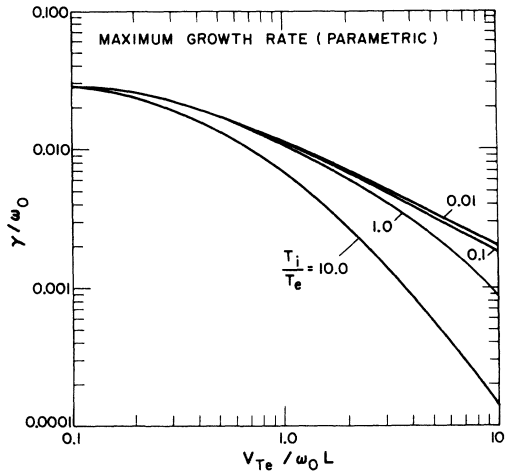

FIG. 6. Maximum growth rates vs $v_{Te}/\omega_0 L$ for the parametric mode.

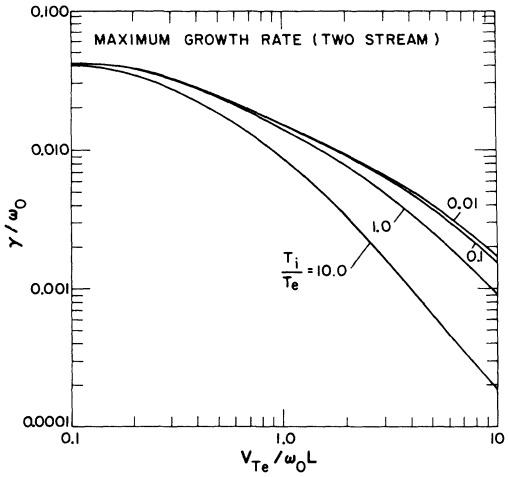

FIG. 7. Maximum growth rates vs $v_{Te}/\omega_0 L$ for the two-stream mode.

IV. TEMPERATURE EFFECTS

To include temperature effects the integral Eq. (2) must be solved. Guided by the form of the solutions in the cold case, we look for solutions of the form

$$\psi(t) = e^{\lambda t} \sum_{n=-\infty}^{\infty} a_n e^{in\omega_0 t} ,$$

where λ is a complex eigenvalue to be determined. Substituting this form into the integral equation leads to the following set of equations for the a_n:

$$\sum_{n=-\infty}^{\infty} G_{mn} a_n = 0 \quad -\infty < m < \infty ,$$

with

$$G_{mn} = \delta_{nm} + \frac{\omega_{pe}^2}{k^2 v_{Te}^2} \sum_{l=-\infty}^{\infty} J_{l+n}\left(\frac{kL}{2}\right) J_{l+m}\left(\frac{kL}{2}\right) \times \left[(-1)^{m+n} Z'\left(\frac{\omega_0(i\lambda + l)}{k v_{Te}}\right) + \frac{T_e}{T_i} Z'\left(\frac{\omega_0(i\lambda + l)}{k v_{Ti}}\right)\right] ,$$

where Z is the plasma dispersion function, δ_{mn} is the δ function, and the J_l are Bessel functions. The system has a solution when

$$\det\left[G_{mn}\left(\lambda, kL, \frac{\omega_p}{\omega_0}, \frac{T_i}{T_e}, \frac{v_{Te}}{\omega_0 L}, \frac{m_e}{m_i}\right)\right] = 0 . \qquad (5)$$

To determine λ we fix the other arguments of G and use a complex numerical root solver. We typically truncate G to a 22×22 matrix and keep 70 terms in the series of each term in solving Eq. (5). We achieve accuracy of better than five significant figures.

Some properties of G_{mn} can be exploited to simplify the calculation. It is clear that

$$G_{mn} = G_{nm}$$

for all values of the parameters. Furthermore, when λ is purely real, as it is for the two-stream mode, it can be shown that

$$G_{mn} = (-1)^{m+n} G^*_{-m-n}$$

and from this it follows that the eigenvalues of G_{mn} occur in conjugate pairs. Thus, for the two-stream mode $\det(G_{mn})$ is real.

The stability properties of the hot plasma have been studied for mass ratio $\mu = \frac{1}{1836}$. Figures 4 and 5 show the $(\omega_p/\omega_0, kL)$ stability diagram for temperature ratio $T_i/T_e = 0.1$ and thermal velocities

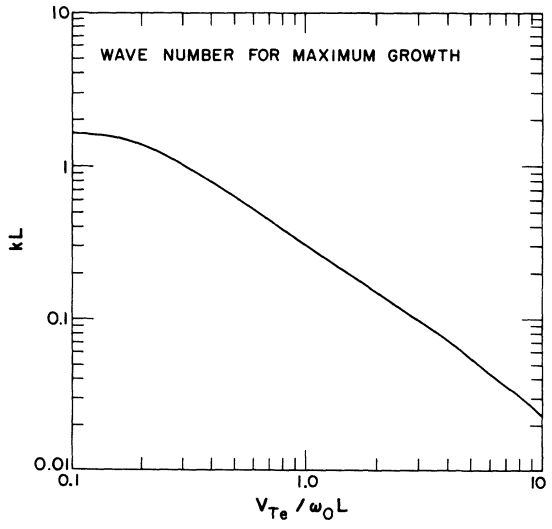

FIG. 8. Wave number of maximum growth for both modes and $0 \le T_i/T_e \le 10$.

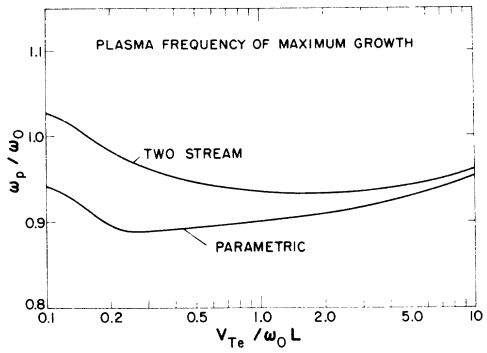

FIG. 9. Plasma frequency of maximum growth for two-stream and parametric modes and $0 \le T_i/T_e \le 10$.

$v_{Te}/\omega_0 L = 0.1$ and 0.5, respectively. Two effects seem to be important in determining the stability regions. First, we no longer have instability at arbitrarily high kL as we observed in the cold case. Rather, all instabilities occur at long wavelengths with the cutoff occurring approximately where $k\lambda_{debye} = 1$. Second, the instability domain extends to lower densities as kL increases, thereby increasing the range of densities over which instability can occur. The boundary between the parametric and two-stream modes is given very nearly by

$$\omega_0^2 = \omega_p^2 + \tfrac{3}{2}(kv_{Te})^2 \quad \text{or} \quad 1 = \left(\frac{\omega_p}{\omega_0}\right)^2 + \frac{3}{2}(kL)^2\left(\frac{v_{Te}}{\omega_0 L}\right)^2 .$$

This is a left-facing hyperbola which passes through the points (1, 0) and $(0, \frac{2}{3}v_{Te}/\omega_0 L)$, and is the well-known Bohm-Gross longitudinal dispersion relation for plasma oscillations. Notice that the two-stream, or overdense; mode has now become unstable *below* the plasma cutoff, which still lies at $\omega_p = \omega_0$. The growth rates are, however, quite low in this region.

In Figs. 6 and 7 we illustrate the maximum growth rate vs thermal velocity for various temperature ratios. Here, the maximum value is obtained by scanning over both the wave number kL and plasma frequency ω_p/ω_0. Figure 6 corresponds to the parametric instability and Fig. 7 to the two-stream instability. Notice that the growth rates fall with increasing $v_{Te}/\omega_0 L$ and T_i/T_e but do not become negative in the range shown; that is there appears to be no high-temperature threshold in this collisionless model as one might expect from the static case. The wave numbers kL corresponding to maximum growth are illustrated in Fig. 8. It turns our that these kL's are nearly independent of T_i/T_e and are almost identical in the two modes so only one curve need be plotted. Again, the kL vs $v_{Te}/\omega_0 L$ is almost linear on the log-log plot indicating a shift to longer wavelengths, but no cutoff. Finally, the plasma frequency at which maximum growth γ occurs is plotted as a function of $v_{Te}/\omega_0 L$ in Fig. 9. These too are virtually independent of T_i/T_e so only one curve for each mode is shown. Despite the fact that the stability diagrams show instabilities at lower plasma frequencies, the maximum growth continues to occur at nearly its cold value.

These curves have very nearly taken on their cold values (Figs. 2 and 3) by $v_{Te}/\omega_0 L = 0.1$. The maximum growth rate of the two-stream mode continues to be about $1\frac{1}{2}$ times that of the parametric mode.

Numerical simulations of this AC two-stream instability by the particle-in-cell method[8,9] have shown good quantitive agreement with the linear growth rates and wavelengths in the case $m_e/m_i = \frac{1}{100}$. The familiar nonlinear development of phase-space vortex structure and coalescing is seen in the electron distribution and to a lesser extent in the ion distribution. However, it is unlikely that the ion turbulence seen with this unphysical mass ratio is qualitatively correct as indicated by Ref. 10. In addition, two or three dimensional effects[9] may be necessary for physically applicable simulations.

ACKNOWLEDGMENTS

The authors would like to thank Drs. C. W. Nielson, D. Forslund, and R. L. Morse for their contributions to the numerical work. This work was performed under the auspices of the U. S. Atomic Energy Commission.

[1]J. P. Silin, Zh. Eksperim. i Teor. Fiz. 48, 1679 (1965) [Sov. Phys. JETP 21, 1127 (1965)].
[2]D. F. Dubois and M. V. Goldman, Phys. Rev. Letters 14, 544 (1965).
[3]E. A. Jackson, Phys. Rev. 153, 235 (1967).
[4]K. Nishikawa, J. Phys. Soc. Japan 24, 916 (1968); 24, 1152 (1968).
[5]P. K. Kaw and J. M. Dawson, Phys. Fluids 12, 2586 (1969).
[6]J. R. Sammartin, Phys. Fluids 13, 1533 (1970).
[7]Margenau and Murphy, *The Mathematics of Physics and Chemistry* (Van Nostrand, New York, 1956).
[8]R. L. Morse and C. W. Nielson, Phys. Fluids 12, 2418 (1969).
[9]R. L. Morse and C. W. Nielson, Phys. Rev. Letters 23, 1087 (1969).
[10]R. L. Morse and C. W. Nielson, Phys. Rev. Letters 26, 3 (1971).